Profilometry with line-field Fourier-domain interferometry

**Takashi Endo, Yoshiaki Yasuno, Shuichi Makita,
Masahide Itoh, and Toyohiko Yatagai**

*Institute of Applied Physics,
University of Tsukuba,
Tennodai 1-1-1, Tsukuba, Ibaraki 305-8573*

endo@optlab2.bk.tsukuba.ac.jp

https://optics.bk.tsukuba.ac.jp/COG/COGWiki/

Abstract: Line-field Fourier-domain interferometry that is capable of a fast three-dimensional (3-D) shape measurement is proposed. This system is constructed from a combination of a conventional Fourier-domain interferometer and a one-dimensional imaging system. This system directs a line-shaped focus onto a specimen, and a two-dimensional shape can be calculated from a single-shot image of the CCD camera without any mechanical scan. An aspherical mirror and a Japanese coin are presented as a 3-D shape measurement example.

OCIS codes: (180.6900) Three-dimensional microscopy; (120.2650) Fringe analysis.

References and links

1. B. S. Lee and T. C. Strand, "Profilometry with a coherence scanning microscope," Appl. Opt. **29**, 3784-3788 (1990).
2. T. Dresel, G. Häusler, and H. Venzke, "Three-dimensional sensing of rough surfaces by coherence radar," Appl. Opt. **31**, 919-925 (1992).
3. G. J. Tearney, B. E. Bouma, S. A. Boppart, B. Golubovic, E. A. Swanson, and J. G. Fujimoto, "Rapid acquisition of *in vivo* biological images by use of optical coherence tomography," Opt. Lett. **21**, 1408-1410 (1996).
4. G. J. Tearney, B. E. Bouma, and J. G. Fujimoto, "High-speed phase- and group-delay scanning with a grating-based phase control delay line," Opt. Lett. **22**, 1811-1813 (1997).
5. P. de Groot and L. Deck, "Three-dimensional imaging by sub-Nyquist sampling of white light interferograms," Opt. Lett. **18**, 1462-1464 (1993).
6. Y. Yasuno, M. Nakama, Y. Sutoh, M. Mori, and T. Yatagai, "Optical coherence tomography by spectral interferometric joint transform correlator," Opt. Commun. **186**, 51-56 (2000).
7. A. F. Zuluaga and R. Richards-Kortum, "Spatially resolved spectral interferometry for determination of subsurface structure," Opt. Lett. **24**, 519-521 (1999).
8. A. B. Vakhtin, K. A. Peterson, W. R. Wood, and D. J. Kane, "Differential spectral interferometry: an imaging technique for biomedical applications," Opt. Lett. **28**, 1332-1334 (2003).
9. M. Born and E. Wolf, *Principles of Optics* (Pergamon Press, New York, 1980).
10. G. Häusler and M. W. Lindner, "Coherence radar and spectral radar—new tools for dermatological diagnosis," J. Biomed. Opt. **3**, 21-31 (1998).
11. M. Wojtkowski, R. Leitgeb, A. Kowalczyk, T. Bajraszewski, and F. Fercher, "In vivo human retinal imaging by Fourier domain optical coherence tomography," J. Biomed. Opt. **7**, 457-463 (2002).
12. C. Dorrer, N. Belabas, J. Likforman, and M. Joffre, "Spectral resolution and sampling issues in Fourier-transform spectral interferometry," J. Opt. Soc. Am. B **17**, 1795-1802 (2000).
13. W. Weise, P. Zinin, T. Wilson, A. Briggs, and S. Boseck, "Imaging of spheres with the confocal scanning optical microscope," Opt. Lett. **21**, 1800-1802 (1996).

14. R. A. Leitgeb, C. K. Hitzenberger, and A. F. Fercher, "Performance of fourier domain vs. time domain optical coherence tomography," Opt. Express, **11**, 889-894 (2003), http://www.opticsexpress.org/abstract.cfm?URI=OPEX-11-8-889.

1. Introduction

White-light interferometry (WLI) [1, 2] is one of the most commonly used methods for three-dimensional (3-D) shape measurements. The WLI setup consists of a Michelson interferometer and a broadband light source. A specimen to be measured is placed at the end of one arm. The specimen and the mirror in each arm reflect the probe and reference light, respectively. These lights are then made to interfere on a detector. An interferogram of the interference fringes contains the height information of the specimen at its peak position.Hence the height can be measured with a resolution of a few micrometers by use of a light source having a bandwidth of a few dozen nanometers. Here the resolution is inversely proportional to the bandwidth of the light source. When compared with monochromatic interferometry, the WLI setup has no phase ambiguity and it permits a wide range of measurement.

As observed, the WLI setup has several advantages: it is noncontact, has high resolution, and has a wide measurement range. These features are required for 3-D shape measurement. However, the problem lies in its measurement time. A mechanical scan consumes the majority of its measurement time. In the WLI setup, we require a mechanical scan of the objective or reference surface in order to obtain one interferogram, and this scan has two restrictions, the first of which is scanning distance. The scanning distance depends on the range of measurement of the height direction, and a long scanning distance is required for a wide measurement range. The second restriction is the sampling interval. The interferogram is constructed by the multiplication of a carrier and an envelope. The center of this envelope indicates the height of the specimen. Hence we require a process that detects the envelope from the interferogram. In this process, the sampling interval of the mechanical scan must be lower than the Nyquist interval of the carrier. In practice, the sampling interval of this restricted scan is estimated to be several tens of nanometers, and therefore the measurement time increases. Although techniques for high-speed mechanical scanning [3, 4] and envelope detection, whose scanning interval is greater than the Nyquist interval [5], have been researched to solve this problem, an additional instrument or an elaborate algorithm is required. Moreover, the problem of the measurement time has not been adequately resolved.

Parallel Fourier-domain optical coherence tomography (FD-OCT) has been introduced [6–8]. We applied this idea to 3-D shape measurement as line-field Fourier-domain interferometry. A spectral interferogram, which includes height information, can be obtained without any mechanical scans. The details are described in Section 2. In addition, we use a one-dimensional (1-D) imaging system to obtain 1-D lateral positioning information. However, a 1-D mechanical scan is required for a 3-D shape measurement. This mechanical scan is along the lateral direction and has no Nyquist restrictions such as with the WLI setup mentioned above.

2. Basic principle of line-field Fourier-domain interferometry

2.1. *Optical scheme*

Figure 1 shows an optical scheme of our line-field Fourier-domain interferometry. This system consists of two parts, an interferometer and a spectrometer, and it is similar to conventional Fourier-domain interferometry, spectral interferometry [9], and FD-OCT [10], except for the cylindrical lens and CCD camera. The cylindrical lens is placed between a light source and a beam splitter. The CCD camera is not a line camera but a two-dimensional (2-D) camera. We define a local coordinate system with the z axis along the direction of propagation of light, and
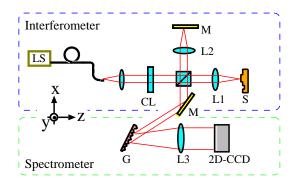
Fig. 1. Optical scheme of the line-field Fourier-domain interferometry. LS, light source. L1, L2, L3 denote spherical lenses of focal length 100, 100, 150 mm, respectively. CL, cylindrical lens of focal length 100 mm. S, specimen. M, mirror. G, grating with 1200 lp/mm
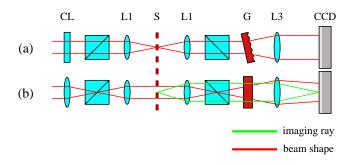

Fig. 2. Perspective of optical setup on (a) the *x-z* plane and (b) the *y-z* plane. CL, cylindrical lens; L1 and L3, lenses; S, specimen; G, grating.

the *x* and *y* axes are in the plane of the page and normal to the plane of the page (pointing out from the page), respectively. Figure 2 shows the perspectives of our system on (a) the *x-z* plane and (b) the *y-z* plane. In this figure, the light for illumination is described on the left-hand side of the specimen, and the backscattered light to a detection is described on the right-hand side.

2.2. *Principle of height measurement*

In this line-field Fourier-domain interferometry, the measurement of the specimen's height, namely, the *z*-axis position, is performed on its *x-z* plane, as shown in Fig. 2(a). The cylindrical lens has no effect on the *x-z* plane; hence this system is considered to be the same as with conventional Fourier-domain interferometry. Here the collimated light is focused on one point of the specimen, and then backscattered light is recollimated and introduced to the spectrometer. Its spectral interferogram is spread along the *x* axis of the CCD camera. The CCD camera detects the intensity of the spectral interferogram, which contains the height information of the specimen.

The spectral interferogram is sampled along the *x* axis with equal wavelength increments. However, this sampling leads to poor resolution along the *z* axis and signal-to-noise ratio (SNR) [11] because the Fourier transform, which is performed in the next process, links time and frequency. To cancel this effect, we replace the equal wavelength sampling with an equal frequency sampling using an interpolation algorithm [12]. Hence the spectral interferogram can

be expressed as a function of frequency as follows:

$$\hat{I}(\omega) = \left|\hat{E}_r(\omega)\right|^2 + \left|\hat{E}_p(\omega)\right|^2 + \hat{E}_r^*(\omega)\hat{E}_p(\omega) + \hat{E}_r(\omega)\hat{E}_p^*(\omega), \tag{1}$$

where E_r and E_p denote the reference and probe light, respectively; $\hat{E}$ denotes the Fourier transform of E; and E^* denotes the complex conjugate of E. The Fourier transform is performed along the x axis in a computer, and the Fourier transform of Eq. (1) is expressed as follows:

$$I(t) = \Gamma[E_r(t)] + \Gamma[E_p(t)] + \Gamma[E_r^*(t), E_p(t)] + \Gamma[E_r(t), E_p^*(t)], \tag{2}$$

where $\Gamma[]$ and $\Gamma[,]$ denote the autocorrelation and cross correlation, respectively. The height information of the specimen is encoded in time in the manner of time of flight. Hence the probe light has a time delay $2h/c$, where h is the height of the specimen and c is the speed of light. We can arrange Eq. (2) as

$$
\begin{aligned}
I(t) &= \Gamma[E_r(t)] + \Gamma\left[E_r\left(t - \frac{2h}{c}\right)\right] \\
&\quad + \Gamma\left[E_r^*(t), E_r\left(t - \frac{2h}{c}\right)\right] + \Gamma\left[E_r^*(t), E_r\left(t - \frac{2h}{c}\right)\right] \\
&= \Gamma[E_r(t)] + \Gamma\left[E_r\left(t - \frac{2h}{c}\right)\right] \\
&\quad + \Gamma[E_r^*(t)] \otimes \delta\left(t - \frac{2h}{c}\right) + \Gamma[E_r^*(t)] \otimes \delta\left(t + \frac{2h}{c}\right),
\end{aligned}
\tag{3}
$$

where $\otimes$ denotes a convolution operator. The first and the second terms of Eq. (3) are the autocorrelations of the reference and probe light, and they appear as a very sharp peak at the center of the calculation result. The third and fourth terms appear at the place shifted from the center, and the amount of shift is proportional to the height of the specimen. Then we designated the center of gravity of the third term or the fourth term as the height of the specimen.

2.3. Extension to a 2-D shape measurement

Subsection 2.2 accounted for the principle of the height measurement. For extension to a 2-D shape measurement, lateral information, which means the 1-D lateral position of the specimen, is required. To obtain this information, we use a 1-D imaging system, and this imaging system is constructed on the y-z plane as shown Fig. 2(b). The light illuminates the specimen with a line-shaped focus, and the specimen is imaged on the CCD camera. Therefore, the lateral information is detected from the y axis of the CCD camera. The single-shot CCD image simultaneously has the height information in its x axis as a spectral interferogram and lateral information in its y axis simultaneously. Hence the 2-D shape of the specimen can be measured from a single-shot CCD image.

2.4. Extension to a 3-D shape measurement

As mentioned, the 2-D shape can be measured using our system without any mechanical scans. An additional 1-D mechanical scan is needed for 3-D shape measurements. This requirement, which implies that the 1-D scan leads to a 3-D shape of the specimen, is similar to WLI using 2-D lateral imaging. However, these scans are completely different. Whereas the scan of the WLI is along the height axis, the scan of our system is along the lateral axis. Hence WLI has the restriction of the Nyquist interval, but our system does not have such a restriction because there is no Nyquist interval in the lateral scan. Therefore a fast mechanical 1-D scan can be easily realized, and our system is thus capable of faster measurement than with WLI.
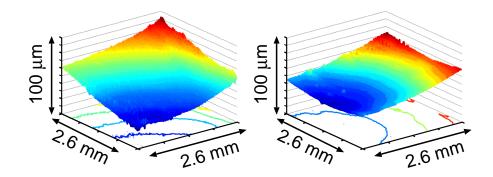
Fig. 3. 3-D shapes of an aspherical mirror. Contour lines are at each 10-μm interval.

Fig. 4. Photograph of a Japanese 10-yen coin. The area of the yellow rectangle is measured using our system.

3.   Prototype system of line-field Fourier-domain interferometry

3.1.   3-D measurement with a prototype system

We constructed a prototype system of the line-field Fourier-domain interferometry. The light source is a superluminescent diode (SLD) whose central wave length is 856 nm and with a FWHM of 24 nm. Our 2-D CCD camera is a visible-IR CCD camera using the NTSC standard, with a frame rate of 30 frames/s (Tokyo Electronic Industry Co., Ltd., Japan). In this system, a stepping motor is used as a mechanical scan to move the specimen along the x axis.

   First, we measured an aspherical mirror. With a confocal microscope, it is difficult to measure the shape of such a mirror, because the mirror can defocus the probe light, which can lead to measurement error [13]. However, in our system, we use only a coherence gate of the light source; hence our measurements are devoid of errors. Here the power of the probe light is less than 500 μW.

   In the next experiment, we measured a Japanese 10-yen coin, as shown in Fig. 4. Also for this measurement, the power of the probe light is less than 500 μW. The coin is made of bronze with a rough surface, and the probe light is scattered by the surface. Figure 5(a) is the result of the 3-D shape measurement, while (b) is the result of a 2-D shape measurement, which is measured from a single-shot CCD image without any mechanical scan. In the case of conventional WLI, a 2-D shape, such as in Fig. 5, cannot be measured without a mechanical scan. In addition, this result indicates that our system has the ability to measure the elaborate shape of a rough surface.
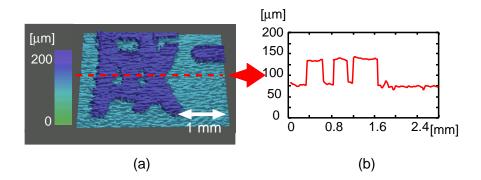
Fig. 5. 3-D and 2-D shapes of a Japanese 10-yen coin.

3.2. Performance of our prototype system

The method for determining resolution in this system is different for each axis. Along the x axis, the spot size of the probe light on the specimen is defined as the resolution. Therefore the resolution depends on the central wavelength of the light source, on the beam diameter, and on the focal length of the objective lens. In the prototype system, the x-axis resolution was theoretically estimated as 16.1 μm. Along the y axis, the optical resolution depends on each instance of Rayleigh resolution for L1 and L3 in Fig. 1. In addition, the pixel size of the CCD camera can limit this optical resolution. In our system, the actual resolution was limited by the pixel size, and it was 9.0 μm. Along the z axis, the resolution is determined as the coherence length. Hence it depends on the spectral width, and the resolution was theoretically 13.5 μm in our system. The precision was 228 nm when the plane mirror was measured. Here the precision denotes the standard deviation of the position of the center of gravity of the peak signals of seven measurements.

The measurement range of the y axis depends on the beam diameter; the magnification of the 1-D imaging system; and the detector size of the CCD camera, which was 2.6 mm for our system. The measurement range of the z axis depends on the resolution of the spectrometer, and the measurement range of our system was 0.8 mm.

Fourier-domain interferometry has an advantage in its SNR as compared with conventional WLI because the signal is added coherently and is reinforced while the noise is added incoherently [14]. In our system, the SNR was 63 dB when we measured the plane mirror, while the shot-noise-limited SNR is theoretically estimated as 72 dB.

With this system, a 2-D shape measurement can be performed without any mechanical scan; therefore the measurement time depends only on the frame rate of the CCD camera. Since the frame rate of our system is 30 frames/s, the measurement time was 1/30 s. In the case of 3-D shape measurement, the measurement time depends not only on the frame rate but also on the speed of the mechanical scan. In the prototype system, the 3-D shape measurement time—such as in Fig. 3, where the volume is 2.6 mm ×2.6 mm ×0.8 mm and the pixel size is 140×140×1024 pixel—was 30 s.

4. Conclusion

We have presented line-field Fourier-domain interferometry as a 3-D shape measurement system, and our Fourier-domain interferometer and 1-D imaging system were constructed on its x-z and y-z planes, respectively. This system does not require any mechanical scan for the 2-D shape measurement, and it is capable of 3-D measurements because a mechanical scan has no

restriction.

Our prototype system requires approximately 30 s for a $140{\times}140{\times}1024$ pixel measurement of 2.6 mm $\times$2.6 mm $\times$0.8 mm volume. This is because almost all the measurement time was used for controlling the stepping motor for one mechanical scan; hence this measurement time is not the principle limit of our system. When a faster mechanical scan system, such as a galvano mirror, is used, this measurement time will be reduced to a few seconds. Indeed, a faster camera, as well, leads to a faster measurement.